



Dynamic Responses of Reinforced Soil Model Wall on Soft Clay Foundation

Sudipta Chakraborty · Ripon Hore · Ayaz Mahmud Shuvon · M. S. Mazhar · Mehedi A. Ansary

Received: 27 August 2019 / Accepted: 11 December 2020 / Published online: 3 January 2021
© The Author(s), under exclusive licence to Springer Nature Switzerland AG part of Springer Nature 2021

Abstract This paper investigated the relative seismic response of reinforced soil retaining wall overlying a soft clayey soil layer—applicable to road or railway embankment. A series of 1D shaking table tests, 0.1 to 0.5 g, were conducted on the 1 m high physical model. The scaled physical model was subjected to harmonic sinusoidal input motions at frequencies of 1 Hz, 3 Hz, 5 Hz, 10 Hz, 12 Hz, and 15 Hz. A laminar box was used to enclose the soil during the experiment. The variation of parameters such as base motion excitations; frequencies; and surcharge pressures were studied. The results of this study revealed that these parameters have a significant

influence on the model wall and vary along the elevation; impacting pore water pressure as well. It also had an impact on the variation along the depth of the clayey soil layer. Maximum face deformation was observed at the top layer of the wall.

Keywords Shake table · Laminar box · Soft clayey soil foundation · Wrap faced reinforced soil wall · Geotextile · Harmonic sinusoidal input motions · Seismic response · Surcharge load

S. Chakraborty · A. M. Shuvon
Bangladesh Network Office for Urban Safety (BNUS),
Bangladesh University of Engineering and Technology,
Dhaka, Bangladesh
e-mail: sudipta.ckr@gmail.com

A. M. Shuvon
e-mail: amshuvon@gmail.com

R. Hore · M. S. Mazhar · M. A. Ansary (✉)
Department of Civil Engineering, Bangladesh University
of Engineering and Technology, Dhaka, Bangladesh
e-mail: ansary@ce.buet.ac.bd

R. Hore
e-mail: riponhore@gmail.com

M. S. Mazhar
e-mail: smazhar@gmail.com

R. Hore
LGED, Dhaka, Bangladesh

1 Introduction

Seismic influence on soil structures played an important role in the area of earthquake geotechnical engineering and was found considerable development in the recent past. Two aspects of model testing were given importance, namely a rigid box, and a laminar box. A laminar box is a sophisticated container than a rigid box which can enhance the accuracy in assessing the ground behavior. In this research, a wrap reinforced soil wall was fabricated on clay soil enclosed by a laminar box and subjected to sinusoidal input motions through the shake table. Moreover, the spacing between the reinforcements and relative density of the backfill were kept constant in all shaking table tests. Based on shaking table tests, this paper attempts to investigate the effect of the frequency and acceleration of the base sinusoidal

motion, surcharge pressure, pore water pressure and the number of layers on the accelerations, horizontal face displacements and soil pressures in wrap-faced retaining walls under simulated seismic conditions. Wrap faced reinforced soil retaining wall on soft clay is popular in all over the world because wrap faced layer consumes less space in both sides of the wall, which is economic and less susceptible to dynamic loading.

According to worldwide experiences, the reinforced soil walls show a flexible behavior and considerable deformation under seismic loads (Edgar et al. 1989; Collin et al. 1992; Ho and Rowe 1996; White and Holtz 1997; Tatsuoka et al. 1995, 1997; Ling et al. 2001). Reinforced soil walls exhibit better performance level when compared to conventional retaining walls under seismic load (Roessing and Sitar 1998). Moreover, the cost of constructions of reinforced soil wall is less than a conventional retaining wall as stated by Latha and Krishna (2006). Many researchers (e.g., Murata et al. 1994; Matsuo et al. 1998; Bathurst et al. 2002; Nimbalkar et al. 2006) studied full scale rigid retaining walls and segmental retaining walls (Nova-Roessig and Sitar 1999; Huang et al. 2003; Ling et al. 2005; Huang and Wu 2006). The practice of wrap-faced reinforced soil increased rapidly worldwide due to its better seismic performance. In spite of its importance, very few studies (e.g., Sakaguchi et al. 1992; Koerner 1999; Perez and Holtz 2004; Benjamim et al. 2007) are available in this regard.

Richardson and Lee (1975) attempted first small-scale shaking table tests on reinforced soil walls with metallic reinforcement. Sakaguchi et al. (1992) and Sakaguchi (1996) carried out shaking table tests on 1.5 m high reinforced model walls and discussed the influence of various parameters. Parameters like relative density of soil, frequency and amplitude of the motion, reinforcement's types, and spacing between the reinforcements, tensile strength and soil interaction, friction angle between reinforcements, facing material, surcharge pressure and others have influence on deformations of the reinforced soil walls under seismic load (Roessing and Sitar 1998; Paulsen 2002). The seismic performance of reinforced soil walls using different reinforcing materials and facing systems were inspected through experimentations and numerical analyses conducted under various

conditions (Richardson et al. 1977; Ling et al. 1997; Matsuo et al. 1998; Koseki et al. 2006; Shahri et al. 2010).

Several shaking table studies were carried out on wrap-faced reinforced soil retaining walls to gain insight into their behavior under dynamic loads was conducted by Latha and Krishna (2006; 2008), Krishna and Latha (2007), Sabermahani et al. (2009) and Esmailabadi et al. (2014). Moreover, a series of laboratory shaking table tests were performed for observing the performance of unreinforced and reinforced soil slopes by Srilatha et al. (2013, 2014) and Latha and Nandhi Varman (2014). Two different slope angles and reinforcement were used in their tests. A reduced-scale shake table test investigating the seismic response of slurry wall and sandy soil was presented by Xiao et al. (2014). Moreover, shaking table tests were performed effectively to investigate the behavior of excess pore water pressure in different soft soil-foundations of soil-structure interaction (SSI) system (Zhang et al. 2009). The performance of geocell retaining walls inside a laminar box under seismic shaking conditions was described by Latha and Manju (2016). Moreover, a series of shaking table tests on 0.9 m high reinforced-soil wall models with different steel strip lengths were performed by Yazdandoust (2017).

This study focuses on the seismic design of roadway or railway embankment on soft clay soil. A scale model testing platform was developed for a single degree of freedom shaking table tests that symbolize the dynamic free-field conditions of clayey soil where a wrapped geotextile-sand retaining wall was erected on clay soil subjected to seismic loading. A total of 90 shaking table tests were carried out on this model embankment. In order to explore the possible influence of the impact on the soil, the test implements repeated loading and unloading process. The effects of frequency, amplitude, surcharge, pore water pressure and displacement along the different elevations were observed in this study.

2 Objective and Scope

The objectives of this study were to (a) observe the behavior of wrap-faced reinforced soil wall under harmonic sinusoidal input motions, (b) fix a suitable scaling for constructing a dummy embankment,

(c) conduct a series of shaking tests effectively, (d) observe the seismic response of the scale model embankment due to alterations in frequency, surcharge and acceleration of base shaking and (e) determine the layer by layer response of soil wall due to these shaking. The specific purpose of the study was to evaluate the seismic response of a constructed embankment model regarding the input of sinusoidal motions.

3 Testing Equipments

3.1 Equipment Used in This Study

3.1.1 Shaking Table

A computer-controlled servo-hydraulic single degree of freedom shaking table facility was used to simulate the horizontal shaking action, associated with seismic and other vibration conditions. The testing platform was made of a 2 m by 2 m size steel base with a 1500 kg of payload capacity as shown in Fig. 1. Shaking was provided by a digitally controlled servo-hydraulic actuator with an acceleration capacity of 0.05 g to 2 g and a frequency range of 0.05 Hz to 50 Hz having a maximum amplitude of ± 200 mm. The total operating system was controlled in a dedicated room.



Fig. 1 Testing platform

3.1.2 Laminar Box

The ideal container is one that gives a seismic response of the soil model identical to that obtained in the prototype. In this study, embankment with soft clayey soil model was constructed in a laminar box to reduce boundary effects. The fabricated laminar shear box consists of 24 hollow aluminum layers of frames. Each layer consists of an inner frame with an inside dimension of 915 mm \times 1220 mm \times 1220 mm. The gap between the successive layers is 2 mm, and the base layer is rigidly connected to the solid aluminum base plate (915 mm \times 1220 mm \times 15 mm).

3.1.3 The Layers

Each layer consists of a rectangular frame with an internal dimension of 1220 mm \times 920 mm \times 50 mm. Transfer ball bearings were used to minimize the friction between the layers. Ball bearings consist of one main ball, with a diameter of 12 mm, placed in a hemispherical space filled with fine balls.

3.1.4 Base Plate and Saturation and Drainage Systems

The lowest layer is fixed on a steel base, rigidly fixed on a steel plate having the same dimension of laminar layers. The base has some space for watering and dewatering via four valves. The area of water entry into the model is covered with porous stone. This arrangement facilitates both the saturation and drainage of the samples.

3.1.5 Membrane

A 2 mm thick rubber membrane, as shown in Fig. 2, was placed inside the laminar box for the hydraulic cut-off system and for the protection of the ball bearings. The significance of using this fabric was that it is designed to fold or unfold as sand moves against it rather than to stretch like a conformist silicone rubber membrane.

3.1.6 Portable Pluviator

Many researchers (e.g., Fretti et al. 1995; Zhao et al. 2006; Choi et al. 2010) attempted in developing



Fig. 2 Membrane is being attached inside the laminar box

methods to control uniformity and to achieve desired relative density (D_r) of sand specimen (Miura and Toki 1982; Rad and Tumay 1987; Lo Presti et al. 1993; Choi et al. 2010; Dave and Dasaka 2012; Srinivasan et al. 2016; Gade and Dasaka 2016). Among these techniques, air pluviation method is preferred because of its advantage to reconstitute uniform sand bed for laboratory testing.

In this study, a portable traveling pluviator developed by Hossain and Ansary (2018), was used to maintain the corresponding relative density of sand layer at 64%. Components of the pluviator are shown in Fig. 3. The physical model was prepared with two soil layers—clayey soil as the lower layer and sandy soil as the upper layer.

4 Materials Used in This Study

4.1 Clayey Soil

The clayey soil sample was collected at a depth of 1.5 m below the existing ground level from a location



Fig. 3 Portable pluviator for construction of the model wall

within BUET, Dhaka city, Bangladesh. This sample was at first oven-dried; subsequently, the dry lumps were powdered gently by using a wooden hammer; and finally sieved through #200 standard sieve to obtain clean clayey soil powder. The particle size distribution of the clean clayey soil is presented in Fig. 4. The specific gravity G_s of the soil was determined, from the laboratory test, to be 2.64. X-ray diffraction tests (XRD) was performed, at a scanning speed of $8^\circ (2\theta) \text{ min}^{-1}$ by using Ni-filtered

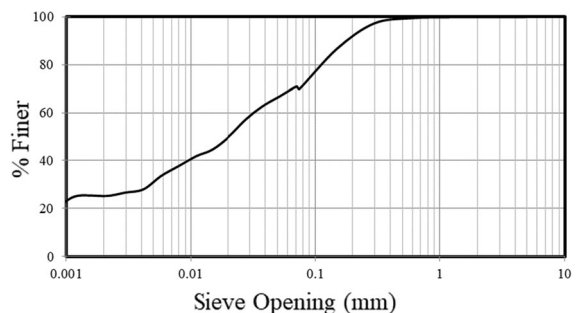


Fig. 4 Grain size distribution of clayey soil

CuK α radiation to identify the mineral composition of clayey soil. XRD test results are summarized in Table 1. A careful examination of these data reveals that the predominant mineralogical composition of the clayey soil was Kaolinite (75%), followed by Illite (25%). An Atterberg limit test was performed on five representative samples. Average liquid limit (LL) and plastic limit (PL) was established to be 41% and 16%, respectively. The soil was defined as Lean Clay (CL), as per USCS classification.

4.1.1 Reconstituted Clayey Soil

Burland (1990) demonstrated that the essential engineering properties of reconstituted clay—shear strength and compressibility—provides a basis to interpret the corresponding properties of the in-situ natural clay soil (regardless of it being normally consolidated or over consolidated). Consequently, in this study, clayey soil was reconstituted by thoroughly mixing the oven-dried clayey soil powder with an initial water content equal to the LL—a procedure described by Burland (1990). The thorough mixing of the slurry was attained with the aid of a ‘Hobart’ rotary mixer. With this slurry, a 610 mm (24 inches) thick reconstituted clayey soil layer was constructed in the laminar shear box; and then consolidated under the

undrained isotropic condition at loads: 15 kPa, 20 kPa, 25 kPa, 30 kPa, 40 kPa, 60 kPa, 80 kPa and 100 kPa, respectively. The consolidation process was observed through the settlement of clayey soil versus time graph, plotted with the aid of calibrated mechanical dial gauges, instrumented on either side of the laminar shear box. The average settlement curve is shown in Fig. 5. This curve shows progressive soil structure collapse, a kind of time dependent bond weakening in the soil. Moreover, pore water pressure dissipates slowly then due to quicker dissipation settlement increases.

UU triaxial test is suitable for saturated clay, silt, peat in both undisturbed and remolded or reconstituted sample for providing the actual field conditions. UU triaxial test was performed on the collected soil sample with a shear rate of 1.5 mm/min for each test. The applied confining stresses for the reconstituted clayey soil samples were 50 kPa and 100 kPa. The obtained value of undrained shear strength (S_u) is 28 kPa.

4.1.2 Sandy Soil

Sand was utilized in the construction of the 0.4 m (16") high reinforced soil zone and backfill soil. The representative sample was oven dried and sieved through ASTM standard sieves (Passing sieve #4 and retaining on #200) to investigate the properties. The resulting particle size distribution is shown in Fig. 6. The coefficient of uniformity (C_u) and the coefficient of curvature (C_c) was 2.19 and 0.68, respectively. The result indicates a poorly graded, medium to fine sand (SP). Fineness modulus of the sand was 2.7. Other physical parameters such as specific gravity (G_s) and maximum dry density (γ_d) had been determined to be 2.65 and 16.6 kN/m³, respectively. The portable traveling pluviator was operated to maintain a target

Table 1 Brief description of XRD test

Compound name	Percent (%) by atomic weight
SiO ₂	67.1747
Al ₂ O ₃	15.8718
Fe ₂ O ₃	7.7982
K ₂ O	3.8247
MgO	1.9221
TiO ₂	1.4624
CaO	0.7423
Na ₂ O	0.6149
P ₂ O ₅	0.1960
SO ₃	0.1568
MnO	0.0960
ZrO ₂	0.0439
Cr ₂ O ₃	0.0339
Rb ₂ O	0.0246
ZnO	0.0205
SrO	0.0171

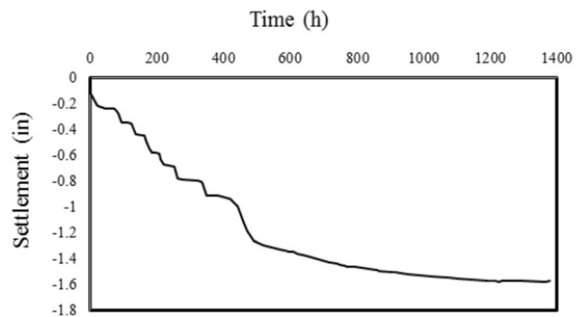


Fig. 5 Average settlement curve

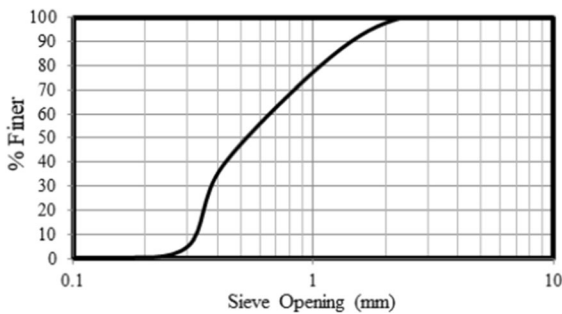


Fig. 6 Grain size distribution of sand

relative density of 64% for the sand layer. This was achieved by ensuring that sand falls from the pluviator at a predetermined constant height for each layer laterally and longitudinally. Strength parameters were determined using the direct shear test. The test establishes an internal angle of friction ϕ of 33°.

4.1.3 Reinforcement

The non-woven polypropylene multifilament geotextile (DF50) was used in reinforcing the sand. Table 2 summarizes the properties of the geotextile. Universal tensile testing machine was used for determining the tensile properties of geotextile. 500 mm × 200 mm sized geotextile sample was taken for this test and the gauge length was 100 mm. Three samples were collected for X and Y direction. Elongation of specimens with increasing load was measured. The load-elongation response of the geotextile was obtained from the wide-width tensile strength test in both X and Y directions. The average initial modulus (E_i) and secant modulus (E_s) in both directions (X and Y) were 40 kN/m, 141 kN/m, and 47 kN/m, 123 kN/m, respectively.

Table 2 Geotextile specification

No	Details	DF 50
1	Reinforcement type	Mechanically bonded needle punched
2	Yarn material (staple fibre)	Polypropylene
3	Mass/unit area (gsm)	322
4	Aperture size, O_{95} (μm)	130
5	Thickness (mm)	2.54
6	Ultimate tensile strength (kN/m)	15.5
7	Ultimate tensile strength at 2% strain (kN/m)	15.97
8	Ultimate tensile strength at 5% strain (kN/m)	16.57

5 Experimental Procedure

5.1 Model Geometry

5.1.1 Height of Clayey Soil Layer

The present study was conducted with a thickness of 610 mm (24 inches) clayey soil layer foundation above which a 50 mm (2 inches) sand blanket was provided as shown in Fig. 7. This clayey soil layer reflects the height limitation of the laminar box and the total weight of the model. Approximately 1 m² geotextile was placed between the clayey soil foundation and sand blanket. The toe boundary of the wall was horizontally free sliding since the wall was constructed on the surface of the foundation. The height of the clayey soil layer of 610 mm (24 inches) was made in three 200 mm (8 inches) stages. Considering the prototype to model scale being $N = 10$ and scale factor $1/N$, the height of the prototype was 6 m (20 ft).

5.1.2 Wall Height and Layers

Wall height is a significant factor governing scale effects and the reaction of the model in contrast with the prototype. Better results were found with the higher height of the sand wall. The average height of traditional walls usually ranges from 4.5 to 5 m (Sabermahani et al. 2009). A 400 mm (16 inches) high model with a scale factor of 10 was fabricated for the current study. Many shake table tests, on the different height of the sand wall, such as 1.5 m (Sakaguchi et al. 1992; Sakaguchi 1996), 1 m (Matsuo et al. 1998; El-Emam and Bathurst 2007), 0.6 m (Krishna and Latha 2007), and 0.33 m (Richardson and Lee 1975) were performed in the past. The schematic geometry of the

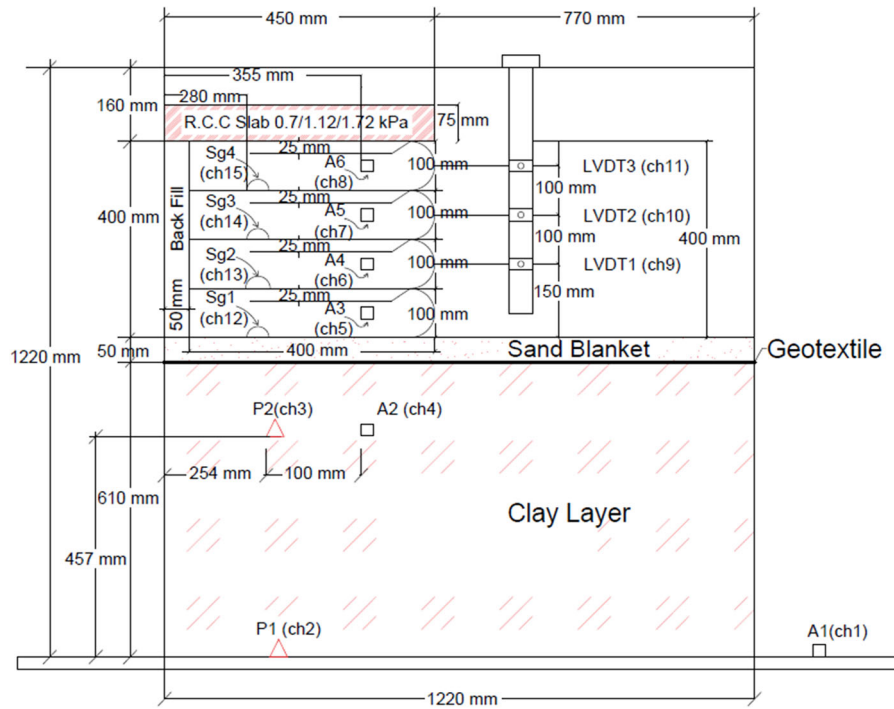


Fig. 7 Schematic illustration of physical model with configuration and instrumentation

experimental model for this study is shown in Fig. 7. The sand wall consists of 4 layers and each layer was 100 mm (4 inches) thick. A concrete block as a surcharge load was placed at the top of the upper layer of the wall after the full construction of four layers.

5.1.3 Facing Type

Wrap-around type wall facing was used with flexible geotextile as shown in Fig. 8. Hence, it allowed free movement of the reinforcing enclosure and had no interaction with the rigid bottom. As per Koerner (1999), each individual facing was formed by wrapping each layer with soft flexible geotextile element. The extended geotextile was anchored by partial burial at the end by backfill material.

5.2 Sensor Arrangement

The accelerations and lateral displacement were measured using accelerometers and displacement transducers (LVDT sensors), respectively at different locations within the clayey soil layer, geotextile wrapped face wall and backfill soil. Six accelerometers (A1, A2, A3, A4, A5, and A6), two pore water

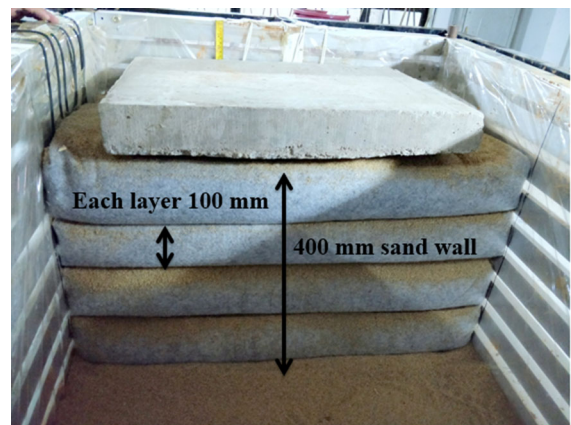


Fig. 8 Finished wrap-faced wall

pressure sensors (P1 and P2), four strain gauges (Sg1, Sg2, Sg3 and Sg4), and three linear variable differential transformers (LVDT1, LVDT2 and LVDT3) were used in this model test. All the sensors were positioned at predefined locations during the layer by layer construction of the physical model. One accelerometer, A1, was fixed to the shake table to record the base acceleration. The other five accelerometers A2, A3, A4, A5, and A6 were placed at elevations 457 mm (18

inches), 710 mm (28 inches), 810 mm (32 inches), 915 mm (36 inches), and 1015 mm (40 inches) mm, respectively, from the base as shown in Fig. 7. A3, A4, A5, and A6 were positioned at a constant distance of 100 mm (4 inches) from the middle of each sand slice. Two pore water pressure sensors; P1 and P2, where P1 was set at the base of the clayey soil layer and P2 was positioned at elevation 457 mm (18 inches) from the base is shown in Fig. 7. The pore water pressure sensor (P2) was placed at a height of 457 mm (18 inches) from the base. However, it was placed to maintain 254 mm (10 inches) horizontal distance from the left face of the laminar box. Strain gauges were attached with geotextile layers. Sg1 was placed at the bottom of the first layer which was just above the sand blanket. However, the other three strain gauges Sg2, Sg3 and Sg4 were placed at elevation 100 mm (4 inches), 200 mm (8 inches), 300 mm (12 inches), respectively from the top surface of the sand blanket as depicted in Fig. 7. Three displacement transducers (LVDT1, LVDT2, and LVDT3) were placed at elevations 150 mm (6 inches), 250 mm (10 inches) and 350 mm (14 inches), respectively from the top of the sand blanket to measure horizontal displacement of the geotextile facings of the top three layers. LVDTs were positioned in place using a hanging T-shaped bracket rigidly connected to the laminar box frame.

5.3 Surcharge Load and Relative Density

A portable pluviator was used in this study to achieve a uniform density of the backfill material as described by Hossain and Ansary (2018). 64% relative density of the backfill soil was achieved by maintaining 200 mm height of fall. The sand which was used for backfill material had been passed ASTM standard sieve number 4 (4.75 mm) and was retained at 200 number sieve (0.075 mm).

Three different surcharge loads 0.7 kPa, 1.12 kPa and 1.72 kPa were employed in this study. The surcharge load was made in the form of a concrete slab. 0.1 g, 0.2 g, 0.3 g, 0.4 g and 0.5 g acceleration based sinusoidal waves were applied to the model for each surcharge load and corresponding measurements were made using the different sensors described before.

5.4 Prototype-Model Similitude

The reliability of model tests depends on whether the model can represent the real behavior of the prototype system. Model size in this study was fixed according to the facilities available for this test. Precise scaling of soil walls and reinforcement properties is needed for considering the stress-dependent behavior of the soil and boundary conditions.

The model is scaled to achieve similitude with the prototype wall. It is not possible to predict the accurate behavior of the prototype with compared to the reinforced model wall using 1 g shaking table test (Krishna and Latha 2007, Latha and Krishna 2008 and Sabermahani et al. 2009). The exponent of confining pressure (α) was assumed to be 0.5 for sand (Kokusho 1980; Yu and Richart, 1984). Considering limitations due to the dimensions of the model container and the capacity of shaking table, the prototype to model scale ratio (N) used was 10 as presented in Table 3.

5.5 Fundamental Frequency

As physical models are shorter versions of prototype walls, the frequency of induced input motions is recommended to scale accurately to produce similar effects to those of earthquakes on prototype walls. It is an essential phase in the seismic design to determine the natural frequencies of the structure.

Reinforced-soil retaining walls of typical heights (i.e., $H > 10$ m) and backfill material are generally considered as short-period structures as addressed by Sabermahani et al. (2009). The response of the wall to ground motion is dominated by the fundamental frequency of the structure (Hatami and Bathurst 2000). The resonant frequency of the walls also changes significantly with the height of the wall (Latha and Krishna 2008). The fundamental frequency of wall model was calculated based on impact test performed before the first shaking of actual tests. The fundamental frequency of the soil embankment model was around 16 Hz. Wall response is critically dependent on the base frequency of the structure, the range of the applied frequencies were kept in a range distant from the fundamental frequency of the walls to avoid resonance which was addressed by Kramer (1996) and Bathurst and Hatami (1998).

Table 3 Scale factors of selected engineering variables (Prototype-Model Similitude)

Description	Parameter	Scale factor	Scale factor M/P	Scale factor P/M
Acceleration	a	1	1	1
Density	ρ	1	1	1
Length	L	1/N	0.10	10
Stress	Σ	1/N	0.10	10
Strain	g	$1/N^{1-\alpha}$	0.32	3.125
Stiffness	G	$1/N^\alpha$	0.32	3.125
Displacement	d	$1/N^{2-\alpha}$	0.031	32.25
Frequency	f	$N^{1-\alpha/2}$	5.62	0.18
Force	F	$1/N^3$	0.001	1000
Force/L	F/L	$1/N^2$	0.01	100
Shear wave velocity	V_s	$1/N^{\alpha/2}$	0.56	1.785
Time	t	$1/N^{1-\alpha/2}$	0.178	5.62

P prototype, *M* model

5.6 Input Motions

Harmonic sinusoidal type of base acceleration was designated for this current parametric study. This harmonic sinusoidal base acceleration is more aggressive than an archetypal earthquake with the same predominant frequency and amplitude which was observed by different researchers in the past (Bathurst and Hatami 1998; Matsuo et al. 1998; El-Emam and Bathurst 2007).

Keeping in mind the fundamental frequency of the embankment model were subjected to 1 Hz, 3 Hz, 5 Hz, 10 Hz, 12 Hz, and 15 Hz frequencies as input motions. The frequency range used in the present study was less than the natural frequency of the system and hence the models were not subjected to resonance. Since frequencies of 2–3 Hz are representative of typical predominant frequencies of medium to high frequency earthquakes (Bathurst and Hatami 1998), the rest of the frequency ranges were used to evaluate the seismic behavior patterns of the existing embankment models. Based on the scale factor of frequency presented in Table 3, these values are respectively corresponding 0.18 Hz, 0.54 Hz, 0.90 Hz, 1.8 Hz, 2.16 Hz and 2.7 Hz frequencies for the prototype. Moreover, the statement is relevant only if the exponent of confining pressure for soil stiffness α is kept equal to 0.5.

A few researchers experimented with base accelerations of low amplitude, such as 0.1 g to 0.2 g (Krishna and Latha 2007; Latha and Manju 2016; Helwany et al. 2017) and some were with high amplitude, such as 0.3 g to 0.5 g (Sabermahani et al.

2009; Edinçliler and Toksoy 2017). In this current research embankment model was subjected to several different excitations from 0.1 g (low amplitude) to 0.5 g (high amplitude) peak base accelerations, each being employed after completion of the previous motion. The duration of each shaking was decided to be kept for at least 5 s. Exactly 90 numbers of harmonic sinusoidal shaking were used for this research as presented in Table 4. All the shaking tests were applied to the newly constructed individual embankment models. A specific base acceleration was achieved through changes in input amplitude for each frequency (1 Hz, 3 Hz, 5 Hz, 10 Hz, 12 Hz, and 15 Hz) and surcharge pressures (0.70 kPa, 1.12 kPa, and 1.72 kPa).

6 Results and Discussion

Results were obtained from several shaking table tests on the embankment model as discussed earlier. The parameters varied in tests were base acceleration, frequency, and surcharge pressure. The base acceleration was kept as 0.1 g, 0.2 g, 0.3 g, 0.4 g, and 0.5 g in different tests as shown in Fig. 9. The range of frequency was varied from 1 to 15 Hz. The surcharge pressure was kept as 0.70 kPa, 1.12 kPa and 1.72 kPa. The thickness of the soft clayey soil layer was 610 mm. Reinforced-soil wall was constructed using sand upon the clayey soil layer in equal lifts (S_v) of 100 mm to achieve a total wall height (H) of 400 mm. The height of clayey soil and reinforced sand wall together including the sand blanket (50 mm thick) had

Table 4 Brief description of ninety tests

Name of tests	Base acceleration a_{\max} (g)	Frequency (Hz)	Input amplitude (mm)	Cycle	Surcharge (kPa)
ST1-ST6	0.1	1, 3, 5, 10, 12 and 15	4.1, 1.61, 1.21, 0.7, 0.67, 0.649	5, 15, 25, 50, 60 and 75	0.70
ST7-ST12	0.2	1, 3, 5, 10, 12 and 15	7.1, 3.12, 2.13, 0.923, 0.905, 0.9506	5, 15, 25, 50, 60 and 75	
ST13-ST18	0.3	1, 3, 5, 10, 12 and 15	11.131, 4.235, 3.123, 1.15, 1.15, 1.225	5, 15, 25, 50, 60 and 75	
ST19-ST24	0.4	1, 3, 5, 10, 12 and 15	14, 5.19, 4.1, 2.13, 2.45, 3.12	5, 15, 25, 50, 60 and 75	
ST25-ST30	0.5	1, 3, 5, 10, 12 and 15	17, 9.65, 5.13, 2.234, 2.367, 2.932	5, 15, 25, 50, 60 and 75	
ST31-ST36	0.1	1, 3, 5, 10, 12 and 15	3.5, 1.3, 0.89, 0.75, 0.75, 0.79	5, 15, 25, 50, 60 and 75	1.12
ST37-ST42	0.2	1, 3, 5, 10, 12 and 15	7, 2.3, 1.65, 1.12, 1.15, 1.12	5, 15, 25, 50, 60 and 75	
ST43-ST48	0.3	1, 3, 5, 10, 12 and 15	10.1, 4.1, 3.35, 1.23, 1.23, 1.26	5, 15, 25, 50, 60 and 75	
ST49-ST54	0.4	1, 3, 5, 10, 12 and 15	14, 5, 3.6, 1.62, 1.78, 1.93	5, 15, 25, 50, 60 and 75	
ST55-ST60	0.5	1, 3, 5, 10, 12 and 15	17, 9.65, 5.13, 1.657, 1.723, 2.1	5, 15, 25, 50, 60 and 75	
ST61-ST66	0.1	1, 3, 5, 10, 12 and 15	4, 2, 1, 0.5, 0.5, 0.65	5, 15, 25, 50, 60 and 75	1.72
ST67-ST72	0.2	1, 3, 5, 10, 12 and 15	6.5, 2.3, 2.2, 0.73, 0.85, 0.93	5, 15, 25, 50, 60 and 75	
ST73-ST78	0.3	1, 3, 5, 10, 12 and 15	10, 4, 2.4, 1.175, 1.36, 1.40	5, 15, 25, 50, 60 and 75	
ST79-ST84	0.4	1, 3, 5, 10, 12 and 15	13, 6, 3.7, 1.65, 1.8, 2	5, 15, 25, 50, 60 and 75	
ST85-ST90	0.5	1, 3, 5, 10, 12 and 15	16, 8.8, 4, 2.55, 1.7, 2.0	5, 15, 25, 50, 60 and 75	

been taken as the full model height (M) which was 1060 mm. The length (L) of the geotextile reinforcement at the interface of the sand layers was kept the same in all tests as 510 mm. The model wall was subjected to 5 to 75 cycles of sinusoidal shaking for obtaining 5 s of data.

6.1 Acceleration Response

Typical time-acceleration histories of the shake table tests ST1, ST7, ST13, ST19 and ST25 with 0.7 kPa surcharge and 0.1 g, 0.2 g, 0.3 g, 0.4 g, and 0.5 g base acceleration and 1 Hz frequency of base sinusoidal motion at same elevation are shown in Fig. 9a–e. Acceleration amplification is the proportion of maximum peak to peak acceleration value in the soil to that of the corresponding value of the base motion. The acceleration amplification profile along the height of the wall for various inputs of base motion after each test of 5 to 75 cycles of sinusoidal motion is presented in Fig. 10a–f. However, to compare the acceleration amplification within the reinforced sand wall, the elevation (z) was represented in non-dimensional shape subsequent to normalizing by the full reinforced sand wall height (H = 400 mm) as can be seen from Fig. 10a–c. On the other hand, to compare

the acceleration amplification between clayey soil layer and reinforced sand wall, the elevation (z) was represented in non-dimensional shape subsequent to normalizing by the height of clayey soil and reinforced sand wall together (M = 1060 mm) as can be seen from Fig. 10d–f. Maximum acceleration amplification was observed almost at the top of the wall in all the tests. This observation was in consensus with the results of physical tests reported by Telekeset al. (1994), Murata et al. (1994) and El-Emam and Bathurst (2005).

6.1.1 Effect of Base Acceleration on Acceleration Amplification in Reinforced Sand Wall

The acceleration amplifications along the height of the wall for different base accelerations of 0.1 g, 0.2 g, 0.3 g, 0.4 g and 0.5 g from ST2, ST8, ST14, ST20, and ST26 tests, respectively, which was conducted at 3 Hz frequency and 0.7 kPa surcharge pressure is presented in Fig. 10a. Acceleration amplifications were found to be higher with increased base accelerations. After analyzing all the test results, it was observed that acceleration amplifications at the top of the wall for 0.1 g and 0.2 g base accelerations were close to 1.11, whereas it was 1.19, 1.29 and 2.01 for

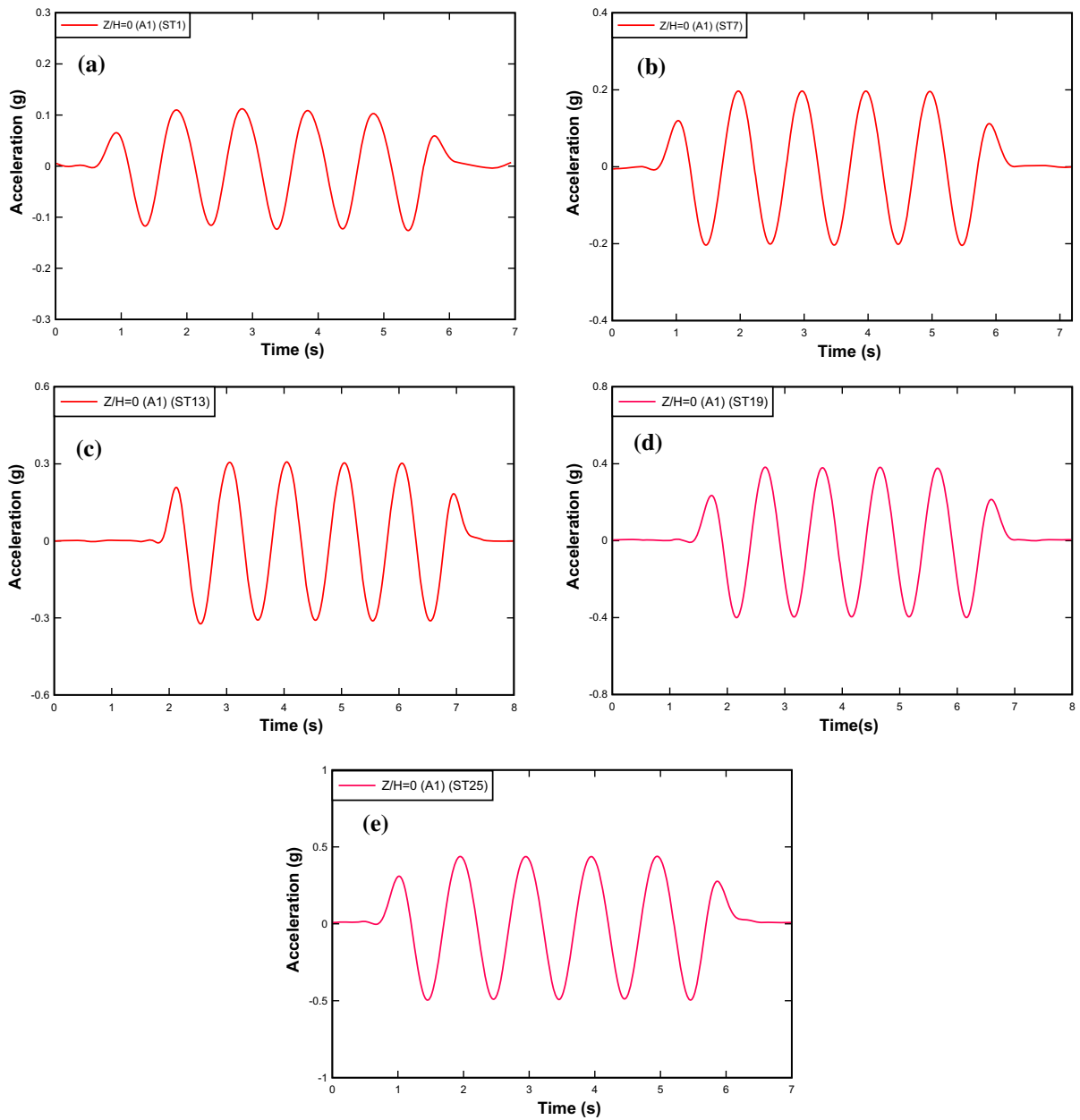


Fig. 9 Input time-acceleration curves (0.1 g to 0.5 g) at frequency 1 Hz

0.3 g, 0.4 g, and 0.5 g base acceleration, respectively. The present study was also compared with the study of Krishna and Latha (2007) as shown in Fig. 10a. The acceleration amplification along the height of the wall for different base accelerations of 0.1 g, 0.15 g and 0.2 g from T4, T6 and T7 model tests (Krishna and Latha 2007) was compared with the present study. In that study, tests were conducted at 2 Hz frequency,

0.5 kPa surcharge, and four layers of reinforcement (total reinforced wall height of 600 mm, each layer thickness was 150 mm). Acceleration amplifications were increased with increased base accelerations for all the curves. However, acceleration amplifications at the top of the wall, for 0.15 g and 0.2 g base accelerations, were very close to 1.70. At the top of the wall, the value of acceleration amplifications was

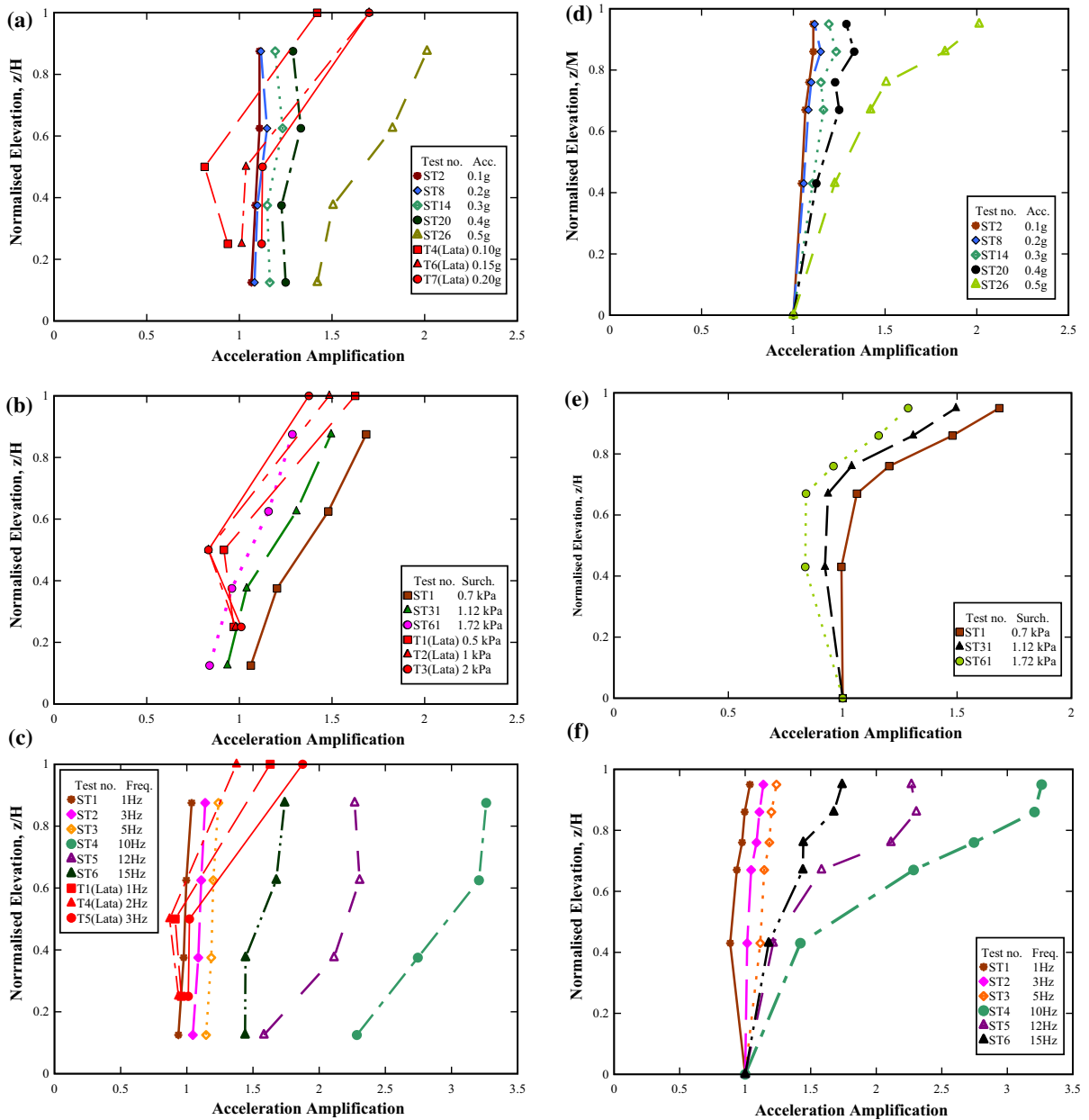


Fig. 10 **a** Effect of base acceleration on acceleration amplification, **b** effect of surcharge on acceleration amplification, **c** effect of frequency on acceleration amplification, **d** effect of base acceleration on acceleration amplification (considering total height of the model including the clay layer for normalization, $M = 1060$ mm), **e** effect of surcharge on

acceleration amplification (considering total height of the model including the clay layer for normalization, $M = 1060$ mm), **f** effect of frequency on acceleration amplification (considering total height of the model including the clay layer for normalization, $M = 1060$ mm)

1.42 for 0.1 g base acceleration. The pattern of amplification for the current study and the study of Krishna and Latha (2007) are almost same. The only difference are observed at the lower part of the curves,

where for the current study, amplification values are relatively high since there is a soft clay layer at the bottom of the reinforced sand wall.

6.1.2 Effect of Surcharge on Acceleration Amplification in Reinforced Sand Wall

Acceleration response against different surcharge pressures was presented from tests ST1, ST31 and ST61 as depicted in Fig. 10b. These tests were conducted with 0.7 kPa, 1.12 kPa and 1.72 kPa surcharge pressures at 1 Hz frequency and 0.1 g base acceleration. Accelerations at the top of the wall were inversely proportional to the surcharge pressures for all the tests. It is observed from the figure that the acceleration amplification values were 1.85, 1.64 and 1.42 for 0.7 kPa, 1.12 kPa and, 1.72 kPa surcharge pressures, respectively. Comparison of the present study with the study of Krishna and Latha (2007) is also shown in Fig. 10b. The acceleration amplifications for 1 Hz frequency and 0.1 g base acceleration along the height of the wall for surcharge pressures of 0.5 kPa, 1.0 kPa and 2.0 kPa from T1, T2, and T3 model tests of Krishna and Latha (2007) was compared with the present study. Accelerations at the top of the wall were inversely proportional to the surcharge pressures, with amplification values of 1.63, 1.47 and 1.37 for 0.5 kPa, 1.0 kPa, and 2.0 kPa surcharge pressures, respectively. The pattern of amplification for the current study and the study of Krishna and Latha (2007) are almost same.

6.1.3 Effect of Frequency on Acceleration Amplification in Reinforced Sand Wall

The effect of frequency on the acceleration response along the height of the wall for tests ST1, ST2, ST3, ST4, ST5 and ST6 with frequencies of 1 Hz, 3 Hz, 5 Hz, 10 Hz, 12 Hz and 15 Hz which were conducted at 0.1 g base acceleration and 0.7 kPa surcharge pressure is shown in Fig. 10c. From the figure, it is observed that the acceleration response against frequency variation is not directly proportional. In fact, within the range of tests conducted accelerations were amplified less for 1 Hz, 3 Hz and 5 Hz and more for 10 Hz and 12 Hz frequencies compared with that of 15 Hz frequency at all elevations. Moreover, accelerations at normalized elevations of 0.125, 0.375, 0.625 and 0.875 were amplified closer or slightly more than 1 for the frequency 1 Hz. The differences in acceleration amplifications for various frequencies were increased with increase in wall height. At a normalized height of 0.875, for 1 Hz, 3 Hz, 5 Hz, 10 Hz, 12 Hz,

and 15 Hz frequency, the values of acceleration amplification were 1.04, 1.24, 1.46, 3.26, 2.47, and 1.80, respectively. Moreover, the acceleration amplification values were 0.94, 0.99, 1.05, 1.51, 1.38 and 1.24 for 1 Hz, 3 Hz, 5 Hz, 10 Hz, 12 Hz, and 15 Hz, respectively at a normalized height of 0.125. These observations highlight the role of the fundamental (resonance) frequency of the system and the proximity of the base excitation frequency (Kramer 1996). Figure 10c also compares the present study with the study of Krishna and Latha (2007). The acceleration amplifications along the height of the wall for different frequency of 1 Hz, 2 Hz and 3 Hz from T1, T4, and T5 model tests of Krishna and Latha (2007) was compared with the present study. These three tests were conducted with the base acceleration of 0.1 g and 0.5 kPa surcharge on the test wall with four layers of reinforcement. The pattern of amplification for the current study and the study of Krishna and Latha (2007) for 1 Hz to 3 Hz frequency are almost same.

6.1.4 Comparison of Acceleration Response between Reinforced Sand Wall and Clayey Soil Layer

To compare the acceleration amplification between clayey soil layer and geotextile wrap faced sand wall, the height of clayey soil and reinforced sand wall together (M) had been taken as the full model height, which is 1060 mm. The acceleration amplifications along the height of the wall for different base accelerations of 0.1 g, 0.2 g, 0.3 g, 0.4 g and 0.5 g from ST2, ST8, ST14, ST20 and ST26 tests, respectively, which were conducted at 3 Hz frequency and 0.7 kPa surcharge is shown in Fig. 10d. From this figure, it is observed that in the clayey soil layer at a normalized elevation of $z/M = 0.43$, the acceleration amplifications were increased with increased base accelerations. It is also observed that in clayey soil layer at $z/M = 0.43$, acceleration amplifies less with compared to the top of the wall ($z/M = 0.95$). At the top of the wall acceleration amplification ranged from 1.11 to 2.01 which were greater than amplification of 1.05 to 1.23 at $z/M = 0.43$.

It is observed that in clayey soil layer at $z/M = 0.43$, for 0.7 kPa, 1.12 kPa and 1.72 kPa surcharge pressures at 1 Hz frequency and 0.1 g base acceleration (from ST1, ST31, and ST61 tests), the acceleration amplitude was 0.99, 0.92, and 0.84,

respectively. Moreover, at the top of the wall, for 0.7 kPa, 1.12 kPa and 1.72 kPa surcharge pressures, the acceleration amplitude values were 1.68, 1.49, and 1.29, respectively as presented in Fig. 10e. Accelerations at the top of the wall were inversely proportional to the surcharge pressures for all the tests, which is logical.

In clayey soil layer at the normalized elevation of 0.43, the acceleration amplitude values were 0.89, 1.07, 0.96, 1.42, 1.21 and 1.18 for 1, 3, 5, 10, 12, and 15 Hz frequencies (from ST1, ST2, ST3, ST4, ST5, and ST6 tests), respectively. However, at the top of the wall ($z/M = 0.95$), for 1 Hz, 3 Hz, 5 Hz, 10 Hz, 12 Hz, and 15 Hz frequencies, the acceleration amplitude values were 0.95, 1.11, 1.17, 3.26, 2.27, and 1.74, respectively as shown in Fig. 10f. The highest acceleration amplitude at top of the wall is for a base input frequency of 10 Hz as can be seen from Fig. 10f. From the figure, it is observed that the acceleration response against frequency variation is not directly proportional.

6.1.5 Displacement Response

Horizontal face displacement along the height of the wall was monitored using three LVDTs positioned as shown in Fig. 7. The displaced face profiles from various tests after 5 to 75 cycles of sinusoidal motion are presented in Fig. 11a–c. Here elevation (z) and horizontal displacements (δh) are presented in non-dimensional form after normalizing them by the height of the wall ($H = 400$ mm).

Figure 11a depicts the normalized displacement profile for different base accelerations of 0.1 g, 0.2 g, 0.3 g, 0.4 g and 0.5 g from tests ST66, ST72, ST78, ST84, and ST90 (as shown in Table 4), respectively. From the figure, it is observed that the normalized displacements were relatively high at higher base accelerations at the normalized elevation of $z/H = 0.875$. This phenomenon had similarity to the test results of Sakaguchi et al. (1992) and Krishna and Latha (2007). A maximum horizontal displacement of 2.11% of the total wall height (H), for 0.5 g, was observed compared with 1.96% for 0.1 g base accelerations. No significant change of displacements had occurred at $z/H = 0.375$ and $z/H = 0.625$ compared to at $z/H = 0.875$.

The normalized displacement profile for tests ST2, ST32, and ST62 after 5 to 75 cycles of base motion,

which were conducted at 0.1 g base acceleration and 3 Hz frequency, were providing an insight into the effect of different surcharge loadings of 0.7 kPa, 1.12 kPa and 1.72 kPa as shown in Fig. 11b. It was observed that the displacement response against surcharge variation was inversely proportional at all elevations. Moreover, this observation was concurrent with the test performed by Krishna and Latha (2007). The maximum displacement of the wall was ($\delta h/H = 2.00\%$) at a surcharge pressure of 0.7 kPa, whereas it was decreased to ($\delta h/H = 1.92\%$) at a surcharge pressure of 1.72 kPa.

According to the Fig. 11c, it can be said that, the displacement response against frequency variation was not directly proportional. The normalized displacement profile observed for tests ST1, ST2, ST3, ST4, ST5, and ST6 with frequencies 1 Hz, 3 Hz, 5 Hz, 10 Hz, 12 Hz, and 15 Hz, respectively, which were conducted at 0.1 g base acceleration and 0.7 kPa surcharge pressure as presented in Fig. 11c. The displacement had occurred more at $z/H = 0.875$ from the range of tests were conducted. The maximum displacement of 2.04% was observed for 12 Hz frequency at $z/H = 0.875$.

6.1.6 Pore Pressure Response

Typical pore water pressure variations obtained from the tests are presented in Fig. 12a–c. The height of clayey soil layer (S) was taken as 610 mm in the case of pore water pressure. The variations of the pore water pressure from model tests ST65, ST71, ST77, ST83, and ST89 with base accelerations 0.1 g, 0.2 g, 0.3 g, 0.4 g, and 0.5 g, respectively for 15 Hz frequency and surcharge load of 1.72 kPa is shown in Fig. 12a. The pore water pressure response against base acceleration variation was directly proportional as can be seen from the figure. The maximum pore water pressure was 0.38 kPa at a base acceleration of 0.5 g. The maximum pore water pressure for model tests ST66, ST72, ST78, ST84, and ST90 was 0.06 kPa, 0.09 kPa, 0.17 kPa, 0.26 kPa, and 0.38 kPa, respectively.

Variations of the pore pressure from model tests ST24, ST54 and ST84 with of surcharge 0.7 kPa, 1.12 kPa and 1.72 kPa, respectively for 15 Hz frequency and base acceleration of 0.4 g is presented in Fig. 12b. From the figure, it is observed that pore water pressure response against surcharge variation

Fig. 11 **a** Effect of base acceleration on displacement profile, **b** effect of surcharge on displacement profile, **c** effect of frequency on displacement profile

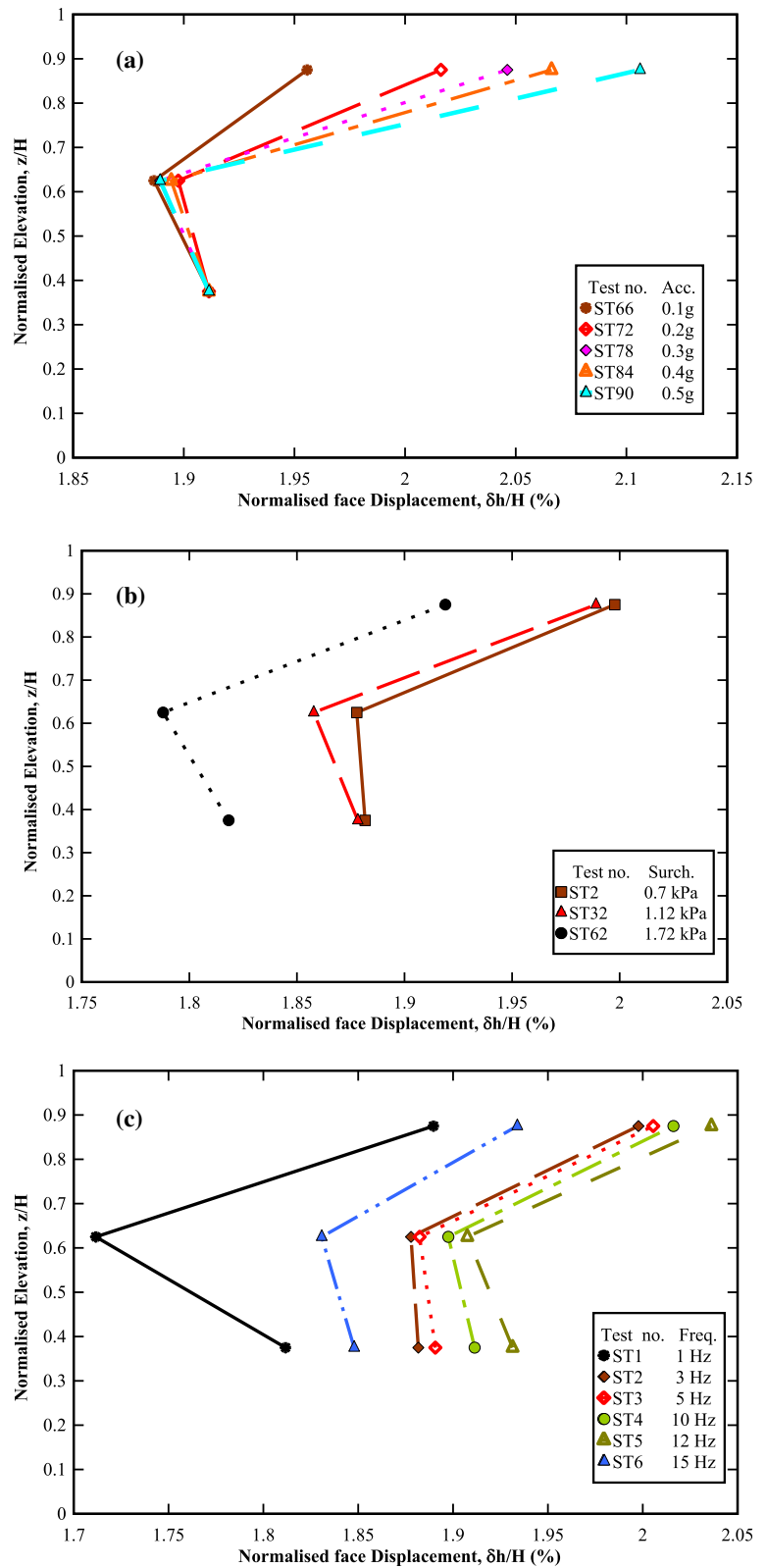
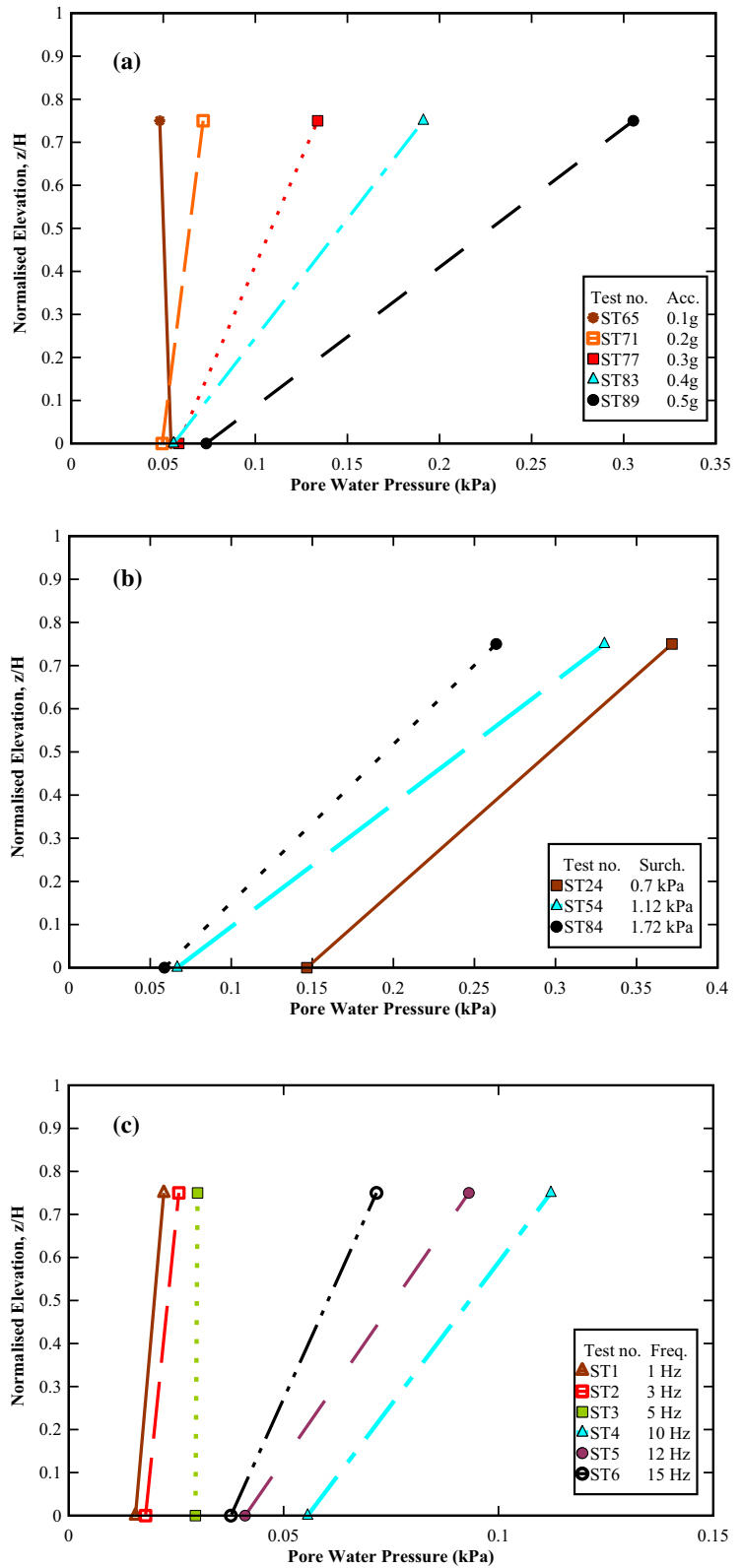


Fig. 12 a Effect of base acceleration on pore water pressure, b effect of surcharge on pore water pressure, c effect of frequency on pore water pressure



was inversely proportional at all elevations. The maximum pore water pressure was 0.37 kPa at a surcharge load of 0.7 kPa. The maximum pore water pressure for model tests ST24, ST54 and ST84 were 0.37 kPa, 0.33 kPa, and 0.26 kPa, respectively.

The effect of frequency for a given base acceleration and surcharge load on pore water pressure for tests ST1, ST2, ST3, ST4, ST5, and ST6 with the frequency of 1 Hz, 3 Hz, 5 Hz, 10 Hz, 12 Hz and 15 Hz for 0.1 g base accelerations and 0.7 kPa surcharge is shown in Fig. 12c. From the figure, it is observed that pore water pressures response against frequency variation is not directly proportional. In fact, pore water pressures increased less for 1 Hz, 3 Hz and 5 Hz and more for 10 Hz, 12 Hz frequencies compared with that of 15 Hz frequencies at all elevations. The highest pore water pressure was 0.105 kPa at 10 Hz frequency.

7 Summary and Conclusions

A series of shaking table studies were carried out on a 1/10 scale model wrap-faced reinforced soil wall to obtain apparent insight into their behavior under harmonic sinusoidal input motions. It was observed that the seismic response of the scale model embankment was significantly affected by changing frequency, and acceleration of base shaking and surcharge loads. Accelerations were amplified both for sand and clayey soil layers, at higher elevations and with high base acceleration. Accelerations were also amplified with low surcharge pressures. It was observed that the acceleration amplification response against frequency variation was not directly proportional. However, the face deformations were high for high base acceleration at the top of the reinforcing layer and impact was relatively low at the other layers. In general, the face deformations were high for low surcharge pressures. It was also observed that the frequency had an inverse impact on face deformations. Pore water pressure gets intensified with increased base acceleration. Increase in surcharge pressure shaking results in a decrease in pore water pressure and the difference being more at higher elevations. These results are helpful to observe the dynamic behavior of the wrap faced soil retaining wall resting on the soft clay layer which is helpful for the design

process of this type of retaining walls considering the seismic environment of Bangladesh.

Authors' Contribution SC: 20%, RH: 40%, AMS: 10%, MFB: 5%, MAA: 25%.

Funding Not applicable.

Availability of Data and Material If requested, we can upload those data.

Code Availability None.

Compliance with Ethical Standards

Conflict of interest The authors declare that there is no conflict of interest.

References

- ASTM D4595. Standard test method for tensile properties of geotextiles by the wide width strip method. ASTM International, West Conshohocken
- Burland JB (1990) On the compressibility and shear strength of natural clays. *Geotechnique* 40(3):329–378
- Bathurst RJ, Hatami K (1998) Seismic response analysis of a geosynthetic reinforced soil retaining wall. *Geosynth Int* 5(1–2):127–166
- Bathurst RJ, El-Emam M, Mashhour MM (2002) Shaking table model study on the dynamic response of reinforced soil walls. In: *Proceedings of the 7th international geosynthetics conference, Nice, France, September 2002*, vol 1, pp 99–102
- Benjamin CVS, Bueno BS, Zornberg JG (2007) Field monitoring and evaluation of geotextile-reinforced soil-retaining walls. *Geosynth Int* 14(2):100–118
- Collin JG, Chouery-Curtis VE, Berg RR (1992) Field observations of reinforced soil structures under seismic loading. In: *Proceedings of international symposium on earth reinforcement*, pp 223–228
- Choi SK, Lee MJ, Choo H, Tumay MT, Lee W (2010) Preparation of a large size granular specimen using a rainer system with a porous plate. *Geotech Test J ASTM* 33(1):1–10
- Dave TN, Dasaka SM (2012) Assessment of portable traveling pluviator to prepare reconstituted sand specimens. *Geomech Eng Int J* 4(2):79–90
- Edgar TV, Puckett JA, D'Spain RB (1989) Effect of geotextiles on lateral pressure and deformation in highway embankments. *Geotext Geomembr* 8:275–292
- El-Emam MM, Bathurst RJ (2005) Facing contribution to seismic response of reduced-scale reinforced soil walls. *Geosynth Int* 12(5):215–238
- El-Emam MM, Bathurst RJ (2007) Influence of reinforcement parameters on the seismic response of reduced-scale

- reinforced soil retaining walls. *Geotext Geomembr* 25(1):33–49
- Esmaeilabadi R, Shahri AA, Behzadafshar K, Gheirati A, Nosrati J (2014) Frequency content analysis of the probable earthquake in Kopet Dagh region-Northeast of Iran. *Arab J Geosci* 8:3833–3844
- Edinçliler A, Toksoy YS (2017) Shake table tests to measure the dynamic performance of geotextile-reinforced embankment. *Period Polytech Civ Eng* 61(4):803–814
- Fretti C, LoPresti DCF, Pedroni S (1995) A pluvial deposition method to reconstitute specimens well graded sand. *Geotech Test J ASTM* 18(2):292–298
- Gade VK, Dasaka SM (2016) Development of a mechanized travelling pluviator to prepare reconstituted uniform sand specimens. *J Mater Civ Eng* 28:04015117
- Ho SK, Rowe RK (1996) Effect of wall geometry on the behavior of reinforced soil walls. *Geotext Geomembr* 14(10):521–541
- Hatami K, Bathurst RJ (2000) Effect of structural design on fundamental frequency of reinforced-soil retaining walls. *Soil Dyn Earthq Eng* 19:137–157
- Huang CC, Chou LH, Tatsuoka F (2003) Seismic displacements of geosynthetic-reinforced soil modular block walls. *Geosynth Int* 10(1):2–23
- Huang C-C, Wu S-H (2006) Simplified approach for assessing seismic displacements of soil-retaining walls. Part I: geosynthetic reinforced modular block walls. *Geosynth Int* 13(6):219–233
- Helwany S, Wu JT, Meinholz P, Alizadeh V, Ghaderi R (2017) Seismic behavior of GRS bridge abutments with concrete block facing: an experimental study. *Transp Infrastruct Geotechnol* 4(4):85–105
- Hossain MZ, Ansary MA (2018) Development of a portable traveling pluviator device and its performance to prepare uniform sand specimens. *Innovative Infrastructure Solutions* 3(1):53
- Kokusho T (1980) Cyclic triaxial test of dynamic soil properties for wide strain range. *Soils Found* 20:45–60
- Kramer SL (1996) *Geotechnical earthquake engineering*. Prentice Hall, Upper Saddle River, NJ, p 653
- Koerner RM (1999) *Designing with geosynthetics*, 4th edn. Prentice Hall, Prentice, p 761
- Koseki J, Bathurst RJ, Güler E, Kuwano J, Maugeri M (2006) Seismic stability of reinforced soil walls: Keynote paper. CD Proceedings of the 8th international conference on geosynthetics, Yokohama, Japan, 18–22 September 2006, pp 28
- Krishna AM, Latha GM (2007) Seismic response of wrap-faced reinforced soil-retaining wall models using shaking table tests. *Geosynth Int* 14(6):355–364
- Lo Presti DCF, Berardi R, Pedroni S, Crippa V (1993) A new traveling sand pluviator to reconstitute specimens of well graded silty sand. *Geotech Test J ASTM* 16(1):18–26
- Ling HI, Mohri Y, Leshchinsky D, Perry EB (1997) Seismic design and performance of geosynthetic-reinforced soil structures. *Geotechnique* 47(5):933–952
- Ling HI, Leshchinsky D, Chou NNS (2001) Post-earthquake investigation on sevealgeosynthetic-reinforced soil retaining walls and slopes during 1999 Ji-Ji earthquake of Taiwan. *Soil Dyn Earthq Eng* 21(4):297–313
- Ling HI, Mohri Y, Leshchinsky D, Christopher B, Matsushima K, Liu H (2005) Large-scale shaking table tests on modular-block reinforced soil retaining walls. *J Geotech Geoenviron Eng* 131(4):465–476
- Latha GM, Krishna AM (2006) Shaking table studies on reinforced soil retaining walls. *Indian Geotech J* 36(4):321–333
- Latha GM, Krishna AM (2008) Seismic response of reinforced soil retaining wall models: influence of backfill relative density. *Geotext Geomembr* 26(4):335–349
- Latha GM, NandhiVarman AM (2014) Shaking table studies on geosynthetic reinforced soil slopes. *Int J Geotech Eng* 8(3):299–306
- Latha GM, Manju GS (2016) Seismic response of geocell retaining walls through shaking table tests. *Int J Geosynth Ground Eng* 2(1):7
- Miura S, Toki S (1982) A sample preparation method and its effect on static and cyclic deformation strength properties of sand. *Soils Found* 22(1):61–77
- Murata O, Tateyama M, Tatsuoka F (1994) Shaking table tests on a large geosynthetic-reinforced soil retaining wall model. In: Tatsuoka F, Leshchinsky D (eds) *Recent case histories of permanent geosynthetic-reinforced soil retaining walls*. Balkema, Rotterdam, pp 259–264
- Matsuo O, Tsutsumi T, Yokoyama K, Saito Y (1998) Shaking table tests and analysis of geosynthetic-reinforced soil retaining walls. *Geosynth Int* 5(1–2):97–126
- Nova-Roessing L, Sitar N (1999) *Centrifuge studies of the seismic performance of reingorced soil structures*. Ph.D. dissertation, University of California, Berkeley
- Nimbalkar SS, Choudhury D, Mandal JN (2006) Seismic stability of reinforced-soil wall by pseudo-dynamic method. *Geosynth Int* 13(3):111–119
- Paulsen SB (2002) *A numerical model for estimating seismic displacements of reinforced steep slopes*. Doctoral dissertation, University of Washington
- Perez A, Holtz RD (2004) Seismic response of reinforced steep soil slopes: results of a shaking table study. In: Yegian MK, Kavazanjian E (eds) *GeoTrans 2004, Proceedings of geotechnical engineering for transportation projects*, 27–31 July, Los Angeles, CA, ASCE Geotechnical Special Publication No. 126, pp 1664–1672
- Richardson GN, Lee KL (1975) Seismic design of reinforced earth walls. *J Geotech Eng Div ASCE* 101(2):167–188
- Richardson GN, Feger D, Fong A, Lee KL (1977) Seismic testing of reinforced earth walls. *J Geotech Eng Div ASCE* 103(1):1–17
- Rad NS, Tumay MT (1987) Factors affecting sand specimen preparation by raining. *Geotech Test J ASTM* 10(1):31–37
- Roessing LN, Sitar N (1998) *Centrifuge studies of the seismic response of reinforced soil slopes*. In: *Third geotechnical engineering and soil dynamic conference, Geotechnical special publication No. 75*, ASCE, pp 458–468, Seattle, Washington
- Sakaguchi M, Muramatsu M, Nagura K (1992) A discussion on reinforced embankment structures having high earthquake resistance. In: *Proceedings of the international symposium on earth reinforcement practice, IS-Kyushu '92*, Fukuoka, Japan, vol 1, pp 287–292

- Sakaguchi M (1996) A study of the seismic behaviour of geosynthetic reinforced walls in Japan. *Geosynth Int* 3(1):13–30
- Sabermahani M, Ghalandarzadeh A, Fakher A (2009) Experimental study on seismic deformation modes of reinforced-soil walls. *Geotext Geomembr* 27(2):121–136
- Shahri AA, Esfandiyari B, Hamzeloo H (2010) Evaluation of a nonlinear seismic geotechnical site response analysis method subject to earthquake vibrations (Case study: Kerman province, Iran). *Arab J Geosci* 4:1103–1116
- Srilatha N, Latha GM, Puttappa CG (2013) Effect of frequency on seismic response of reinforced soil slopes in shaking table tests. *Geotext Geomembr* 36:27–32
- Srilatha N, Latha GM, Puttappa CG (2014) Shaking table studies on geotextile reinforced soil slopes, Golden Jubilee conference of the IGS Bangalore chapter, geo-innovations, 30–31 October 2014, pp 1–8
- Srinivasan V, Srivastava S, Ghosh P (2016) Optimization and parametrical investigation to assess the reconstitution of different types of Indian sand using portable travelling pluviator. *Geotech Geol Eng* 34(1):59–73
- Tatsuoka F, Tateyama M, Koseki J (1995) Behavior of geogrid-reinforced soil retaining walls during the great Hanshin-Awaji earthquake. In: *Proceedings of 1st international symposium earthquake geotechnical engineering*, vol 2, pp 55–60
- Telekes G, Sugimoto M, Agawa S (1994) Shaking table tests on reinforced embankment models. In: *Proceedings of the 13th international conference on soil mechanics and foundation engineering*, New Delhi, India, vol 2, pp 649–654
- Tatsuoka F, Koseki J, Tateyama M (1997) Performance reinforced soil structures during the 1995 Hyogo-ken Nambu earthquake. In: Ochiai H, Yasufuku N, Omine K (eds) *Earthquake reinforcement*. Balkema, Rotterdam, pp 979–1008
- White D, Holtz RD (1997) Performance o geosynthetic reinforced slopes and walls during the Nothridge California earthquake of January 17, 1994. In: Ochiai H, Yasufuku N, Omine K (eds) *Earth reinforcement*. Balkema, Rotterdam, pp 965–972
- Xiao M, Ledezma M, Hartman C (2014) Shake table test to investigate seismic response of a slurry wall. In: *Gecongress 2014: geo-characterization and modeling for sustainability*, pp 1234–1243
- Yazdandoust M (2017) Investigation on the seismic performance of steel-strip reinforced-soil retaining walls using shaking table test. *Soil Dyn Earthq Eng* 97:216–232
- Yu P, Richart FE (1984) Stress ratio effects on shear modulus of dry sands. *J Geotech Eng ASCE* 110(GT3):331–345
- Zhao Y, Gafar K, Elshafie MZEB, Deeks AD, Knappett JA, Madabushi SPG (2006) Calibration and use of new automatic sand pourer. In: *Sixth international conference on physical modeling in geotechnics*, Hong Kong. Taylor and Francis, London, pp 265–270, 4–6 Aug 2006
- Zhang Z, Cho C, Pan Q, Lu X (2009) Experimental investigation on excess pore water pressure in soft soil-foundations under minor shocks. *Int J Eng Appl Sci* 5(4):259–263

Publisher's Note Springer Nature remains neutral with regard to jurisdictional claims in published maps and institutional affiliations.